

Article

Pollution Characteristics of Water-Soluble Inorganic Ions in PM_{2.5} from a Mountainous City in Southwest China

Yimin Huang¹, Liuyi Zhang^{1,2,*}, Chao Peng², Yang Chen², Tingzhen Li¹ and Fumo Yang^{1,2,3,*}

¹ Chongqing Key Laboratory of Water Environment Evolution and Pollution Control in Three Gorges Reservoir, Chongqing Three Gorges University, Chongqing 404000, China

² CAS Key Laboratory of Reservoir Environment, Chongqing Institute of Green and Intelligent Technology, Chinese Academy of Sciences, Chongqing 400714, China

³ National Engineering Research Center for Flue Gas Desulfurization, Department of Environmental Science and Engineering, Sichuan University, Chengdu 610065, China

* Correspondence: zhangliuyi@sanxiau.edu.cn (L.Z.); fmyang@scu.edu.cn (F.Y.)

Abstract: In order to explore the characteristics of water-soluble inorganic ions (WSIIs) in the atmosphere of Wanzhou, a small mountainous city in Chongqing, four representative seasonal PM_{2.5} samples and gaseous precursors (SO₂ and NO₂) were collected from April 2016 to January 2017. The WSIIs (including Cl⁻, NO₃⁻, SO₄²⁻, Na⁺, NH₄⁺, K⁺, Mg²⁺, and Ca²⁺) were analyzed by ion chromatography. During the sampling period, daily PM_{2.5} concentration varied from 3.47 to 156.30 μg·m⁻³, with an average value of 33.38 μg·m⁻³, which was lower than the second-level annual limit of NAAQS-China. WSIIs accounted for 55.6% of PM_{2.5}, and 83.1% of them were secondary inorganic ions (SNA, including SO₄²⁻, NO₃⁻, and NH₄⁺). The seasonal variations of PM_{2.5} and WSIIs were similar, with the minimum in summer and the maximum in winter. PM_{2.5} samples were the most alkaline in summer, weakly alkaline in spring and winter, and close to neutral in fall. The annual average ratio of NO₃⁻/SO₄²⁻ was 0.54, indicating predominant stationary sources for SNA in Wanzhou. NO₃⁻, SO₄²⁻, and NH₄⁺ mainly existed in the form of (NH₄)₂SO₄ and NH₄NO₃. The results of the principal component analysis (PCA) showed that the major sources of WSIIs in Wanzhou were the mixture of secondary inorganic aerosols, coal combustion, automobile exhaust (49.53%), dust (23.16%), and agriculture activities (9.68%). The results of the backward trajectory analysis showed that aerosol pollution in Wanzhou was mainly caused by local emissions. The enhanced formation of SNA through homogeneous and heterogeneous reactions contributed to the winter PM_{2.5} pollution event in Wanzhou.

Keywords: PM_{2.5}; water-soluble inorganic ions; source apportionment



Citation: Huang, Y.; Zhang, L.; Peng, C.; Chen, Y.; Li, T.; Yang, F. Pollution Characteristics of Water-Soluble Inorganic Ions in PM_{2.5} from a Mountainous City in Southwest China. *Atmosphere* **2022**, *13*, 1713. <https://doi.org/10.3390/atmos13101713>

Academic Editor: Yoshiteru Iinuma

Received: 29 September 2022

Accepted: 17 October 2022

Published: 18 October 2022

Publisher's Note: MDPI stays neutral with regard to jurisdictional claims in published maps and institutional affiliations.



Copyright: © 2022 by the authors. Licensee MDPI, Basel, Switzerland. This article is an open access article distributed under the terms and conditions of the Creative Commons Attribution (CC BY) license (<https://creativecommons.org/licenses/by/4.0/>).

1. Introduction

Atmospheric fine particulate matter (PM_{2.5}, with aerodynamic diameter ≤ 2.5 μm particulate matter) is one of the primary air pollutants in most cities [1,2]. Due to the characteristics of small particle size, higher surface/mass ratio, and easy retention in the air, PM_{2.5} easily becomes the reactant and carrier of other pollutants, thus enriching more harmful chemical components [3]. Chemical components of PM_{2.5} include organic carbon (OC), elemental carbon (EC), water-soluble inorganic ions (WSIIs), crustal elements, and various trace elements. WSIIs are the main components of PM_{2.5}, which affect the formation of cloud condensation nuclei, atmospheric extinction coefficient, atmospheric radiation balance, and precipitation acidity, and harm human health [4–6]. Secondary inorganic ions (SNA, including SO₄²⁻, NO₃⁻, and NH₄⁺) are the dominant components, usually accounting for 50%~90% of WSIIs [5,7–9]. In addition, studies showed that the proportion of SNA increased significantly during severe haze periods, indicating that they play a crucial role in haze formation and visibility impairment [10–13].

Many studies related to PM_{2.5} and WSIs have focused on large or megacities in China, such as Beijing, Shanghai, Guangzhou, and Tianjin [11,14–16]. Those studies showed that the concentration of WSIs was mainly determined by local emissions and regional transportation, and meteorological conditions (e.g., temperature, humidity, wind speed, etc.) can also affect the distribution and pollution characteristics of WSIs through chemical processes and physical diffusion. From the perspective of spatial distribution, the concentrations of WSIs in the Beijing–Tianjin–Hebei area (BTH) [2,17,18], Fenwei Plain [1,19], and Sichuan Basin [5,9] were higher than those in the Pearl River Delta (PRD) [20,21] and coastal region [22,23] in China. In terms of inter-annual variation, PM_{2.5} concentrations in major cities have shown a downward trend since the Chinese government issued the Air Pollution Prevention and Control Action Plan (APPCAP) in 2013 [24]. The composition proportion of WSIs in PM_{2.5} and source contributions of WSIs varied remarkably. For example, many studies showed that the concentration of SO₄^{2−} had a declining trend in recent years due to strict strategies implemented in China, such as installing desulphurization systems in coal-fired power plants and conversion of fuel to natural gas [5,25,26]. However, the concentration of NO₃[−] was found to have an increasing trend; therefore, a transition from sulfate-driven to nitrate-driven aerosol pollution appeared in some cities [26–29]. In terms of seasonal variation, the highest concentrations of PM_{2.5} and its WSIs were mostly observed in the cold seasons regardless of geographical regions in China. In winter, the enhanced emissions of coal combustion and biomass burning, as well as stagnant meteorological conditions, such as low wind speed and high relative humidity, were responsible for PM_{2.5} pollution [24,30–33].

Wanzhou, as an important transportation hub city, is located in the border area of six provinces and cities, namely northeast Chongqing, northeast Sichuan, southern Shaanxi, western Hubei, western Hunan, and northern Guizhou. It is also the eastern opening gateway of the Chengdu–Chongqing twin city economic circle and the regional center city of northeast Chongqing Three Gorges Reservoir Area town group. It has high relative humidity and low wind speed all year round, which makes the air pollution in this area more serious [34]. Previous studies on air pollution in Wanzhou were all about PM_{2.5} and its carbonaceous components. For example, Zhang et al. (2015) found that annual average PM_{2.5} concentrations were 125.3 µg·m^{−3} in 2013 in Wanzhou, which was 3.6 times higher than the National Ambient Air Quality Standards of China (NAAQS-China, annual limit of 35 µg·m^{−3}) [35]. Huang et al. (2020) found annual fine particle black carbon (BC) mean displayed a significantly decreasing trend in Wanzhou since the implementation of APPCAP, from 5.3 µg·m^{−3} in 2013 to 3.7 µg·m^{−3} in 2017 [36]. However, the characteristics of WSIs in Wanzhou are still unknown. In order to provide effective guidance for local governments to formulate pollution prevention and control policies for PM_{2.5}, a comprehensive sampling of PM_{2.5} was conducted in Wanzhou from April 2016 to January 2017 to obtain the concentration data of WSIs in PM_{2.5}. In this study, WSIs' mass concentration level and seasonal variation characteristics were firstly analyzed. Then, the chemical forms of main secondary ions and their formation mechanisms were discussed. Finally, the main sources of PM_{2.5} were identified through principal component analysis (PCA). In addition, the formation mechanism of an air pollution event that occurred in winter was explored in this study.

2. Materials and Methods

2.1. PM_{2.5} Sampling

PM_{2.5} samples were collected on a rooftop of the experimental building about 27 m above the ground (30.79° N, 108.37° E) within the Chongqing Three Georges University (Figure 1) in Wanzhou, a small urban city located about 228 km northeast of the megacity Chongqing. The monitoring site is surrounded by residential and commercial areas, agricultural fields, and a main traffic road (Shalong road). There is no fixed atmospheric pollution source within 1 km of the sampling site.

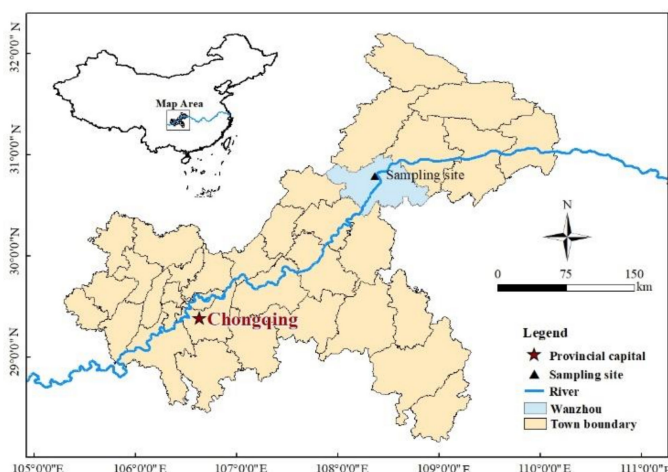


Figure 1. Location of sampling site.

Two $PM_{2.5}$ samples were collected in parallel by one sampler (URG-3000K, URG Corp., Carrboro, NC, USA) with a flow rate of $15\text{ L}\cdot\text{min}^{-1}$. The left channel was connected with an annular denuder and Teflon filter (diameter 47 mm), while the right channel was connected with a quartz filter (diameter 47 mm). $PM_{2.5}$ mass was the sum of the weight of the Teflon filter and quartz filter (after deducting the mass of the blank filters) and then divided by the sum of the volume of the left and right channels. $PM_{2.5}$ samples were collected for 30 days in each of the four seasons: spring (8 April to 7 May 2016); summer (7 July to 5 August 2016); fall (14 October to 12 November 2016); winter (18 December 2016 to 16 January 2017). The sampling duration was 23 h per day, from 11:00 am to 10:00 am (the next day). A total of 120 days of $PM_{2.5}$ samples were collected. The annular denuder was wetted with glycerol/citric acid solution to absorb NH_3 from the air. Hourly concentrations of NO_2 and SO_2 were measured by on-line gas analyzers, including Thermo 42i NO_2 and 43i SO_2 analyzers (Thermo Scientific Corp., Waltham, MA, USA). NO_2 and SO_2 were averaged in the same periods as $PM_{2.5}$. At the same time, the meteorological parameters were also collected by weather stations (WS500-UMB, Lufft Corp., Fellbach, Germany) during the sampling period, and the main meteorological parameters and air pollutant concentrations are listed in Table 1.

Table 1. Meteorological data and air pollutant concentrations during the sampling period.

Season	T/(°C)	RH/(%)	WS/($\text{m}\cdot\text{s}^{-1}$)	Radiation/($\text{W}\cdot\text{m}^{-2}$)	NH_3 /($\mu\text{g}\cdot\text{m}^{-3}$)	NO_2 /($\mu\text{g}\cdot\text{m}^{-3}$)	SO_2 /($\mu\text{g}\cdot\text{m}^{-3}$)
Spring	20.61	76.62	0.95	151.18	18.86	44.38	8.55
Summer	30.03	68.28	1.01	226.82	14.57	23.60	12.40
Fall	17.41	83.30	0.73	65.87	11.98	31.63	13.23
Winter	10.41	76.90	0.74	36.97	11.65	42.27	15.67
Annual	19.69	76.27	0.86	120.89	14.49	38.37	12.49

T, temperature; WS, wind speed; RH, relative humidity.

2.2. Ions Analysis

The adsorbed NH_3 was eluted with ultrapure water, and the eluent was then filtered by a $0.45\mu\text{m}$ poresyringe filter. $PM_{2.5}$ samples were ultrasonically extracted with ultrapure water, and then the extracted solution was filtered by a $0.45\mu\text{m}$ poresyringe filter. Eight WSIs, including SO_4^{2-} , NO_3^- , Cl^- , Na^+ , NH_4^+ , K^+ , Mg^{2+} , and Ca^{2+} , were determined using ion chromatography (Dionex-600, Dionex Corp., Sunnyvale, CA, USA). The cationic column CS12A and anionic column AS11-HC were used for sample analysis. The eluent used for the determination of cations was $20\text{ mmol}\cdot\text{L}^{-1}$ MSA (methanesulfonic acid) at a flow rate of $1\text{ mL}\cdot\text{min}^{-1}$. The anionic eluent was $30\text{ mmol}\cdot\text{L}^{-1}$ KOH at a flow rate of $1\text{ mL}\cdot\text{min}^{-1}$. The reference materials were prepared with the anionic and cationic standard

solutions of O₂Si from the United States, and the correlation coefficient of each standard curve can reach 0.999. Blank and standard samples were repeated every ten samples.

3. Results and Discussion

3.1. Concentrations of PM_{2.5} and WSIs

During the sampling period, daily PM_{2.5} concentration varied from 3.47 to 156.30 $\mu\text{g}\cdot\text{m}^{-3}$ with an average value of 33.38 $\mu\text{g}\cdot\text{m}^{-3}$, which was lower than the NAAQS-China (annual limit of 35 $\mu\text{g}\cdot\text{m}^{-3}$). The PM_{2.5} concentration in Wanzhou was significantly lower than that in Chongqing urban areas such as Fuling, Yubei, and Beibei and lower than that in Jin Yun mountain, a rural background of Chongqing. (Table 2). In addition, compared with other cities in China, it was much lower than Handan, Taiyuan, Chengdu, and Neijiang and comparable to Nanning and Kunming. In general, the PM_{2.5} concentration in Wanzhou is relatively low in China. It is worth noting that the annual average PM_{2.5} concentration in this study decreased by 73.4% compared to the previous report in 2013 [35]. Since the implementation of the APPCAP in 2013, the Chongqing municipal government has taken a series of corresponding measures to improve the city's air quality, such as eliminating yellow-labeled vehicles, installing desulphurization systems in coal-fired power plants, controlling dust pollution, and banning the open burning of straw and garbage. These measures have effectively reduced the atmospheric particulate matter concentration in Chongqing. We also found from the literature that the atmospheric particulate matter concentration in other districts of Chongqing has also decreased in recent years. For instance, Chen et al. (2019) found that the PM_{2.5} level decreased by 57.3% in 2012–2013 compared to that in 2005–2006 in Yubei, Chongqing. The PM_{2.5} concentration decreased by nearly 66% and 40% in 2017–2018 compared to that in 2005–2006 and in 2014–2015 in Beibei, Chongqing, respectively [7].

Table 2. Comparison of water-soluble inorganic ion (WSII) concentrations ($\mu\text{g}\cdot\text{m}^{-3}$) in Wanzhou to other cities in China.

City	Sampling Time	Na ⁺	NH ₄ ⁺	K ⁺	Mg ²⁺	Ca ²⁺	Cl ⁻	SO ₄ ²⁻	NO ₃ ⁻	WSIs	PM _{2.5}	Reference
Wanzhou	2016.04–2017.01	1.48	3.66	0.38	0.10	0.48	0.66	7.53	4.05	18.34	33.16	This study
Fuling, Chongqing	2015.04–2016.01		6.80	0.57			1.00	13.70	6.70	28.77	66.90	[37]
Yubei, Chongqing	2015.12–2016.03	0.28	6.56	1.17	0.35	0.28	1.35	17.5	10.9	38.4	67.54	[5]
Beibei, Chongqing	2017.09–2018.08	0.22	4.87	0.87	0.07	1.51	0.90	9.81	7.36	25.61	43.02	[7]
Jin Yun mountain, Chongqing	2014.10–2015.07		5.5	0.48				12.2	5.6	24.8	56.2	[38]
Chengdu	2012–2013	0.45	9.0	1.23	0.07	0.44	2.46	17.7	11.9	43.0	86.7	[39]
Neijiang		0.21	8.2	1.17	0.06	0.32	0.69	17.6	7.8	35.4	78.6	
Nanning	2017.09–2018.08	0.19	3.23	0.61	0.08	2.31	0.44	9.14	3.08	19.08	37.02	[40]
Handan	2013	0.7	13	1.8	0.1	1	4.4	25.2	20.6	66.80	131	[18]
Kunming	2017.09–2018.08	0.13	2.53	0.44	0.09	2.49	0.51	6.84	2.37	15.40	30.27	[41]
Taiyuan	2015.08–2016.05	0.5	12.7	1.3	0.8	2.6	3.4	19.1	13.1	53.2	109.6	[42]
Xiangtan	2016.04–2017.01		5.6				2.8	14.4	9.6	40.9	73.6	[43]

Daily WSIs concentrations ranged from 3.59 to 106.99 $\mu\text{g}\cdot\text{m}^{-3}$, with an annual average concentration of 18.34 $\mu\text{g}\cdot\text{m}^{-3}$, accounting for 55.6% of PM_{2.5} mass. This concentration was obviously lower than in other districts of Chongqing, slightly higher than Kunming, and only about 1/3 of WSIs concentration in Handan and Taiyuan (Table 2). The order of annual average concentrations of the eight ions is SO₄²⁻ > NO₃⁻ > NH₄⁺ > Na⁺ > Cl⁻ > Ca²⁺ > K⁺ > Mg²⁺. SO₄²⁻, NO₃⁻, and NH₄⁺ (SNA) were the most abundant components of WSIs, accounting for 41.1%, 22.1%, and 19.9% of total WSIs (TWSIs), respectively.

3.2. Seasonal Variations of PM_{2.5} and WSIs

Figure 2 displays the seasonal variation of PM_{2.5} with the maximum in winter (59.82 $\mu\text{g}\cdot\text{m}^{-3}$), decreasing through spring (30.87 $\mu\text{g}\cdot\text{m}^{-3}$) and fall (25.20 $\mu\text{g}\cdot\text{m}^{-3}$), and the minimum in

summer ($17.61 \mu\text{g}\cdot\text{m}^{-3}$), which was consistent with that reported at a different site of Chongqing [9]. The pollution of $\text{PM}_{2.5}$ was the most serious in winter, with a concentration of 3.4 times that in summer. The number of days exceeding the NAAQS-China daily limit of $75 \mu\text{g}\cdot\text{m}^{-3}$ was 26.7% in winter, while in other seasons, it did not exceed the standard. Stagnant meteorological conditions and biomass burning by residents to keep themselves warm were the major causes of the highest $\text{PM}_{2.5}$ mass in winter, while the lower $\text{PM}_{2.5}$ mass concentration in summer was mainly due to abundant precipitation favoring wet scavenging [44].

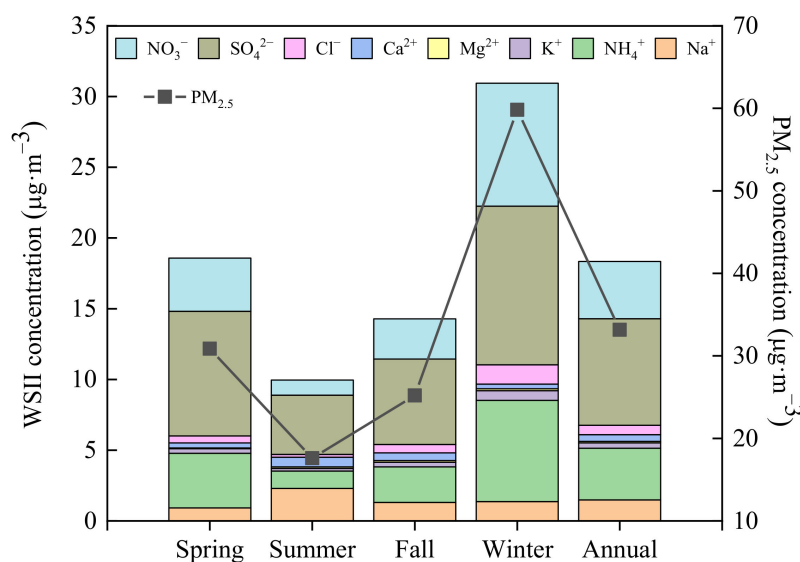


Figure 2. Seasonal variations of $\text{PM}_{2.5}$ and WSIs.

The seasonal variation of TWSIs concentration was similar to $\text{PM}_{2.5}$ mass, and the order was winter ($30.94 \mu\text{g}\cdot\text{m}^{-3}$) > spring ($18.58 \mu\text{g}\cdot\text{m}^{-3}$) > fall ($14.28 \mu\text{g}\cdot\text{m}^{-3}$) > summer ($9.96 \mu\text{g}\cdot\text{m}^{-3}$). The proportion of WSIs in $\text{PM}_{2.5}$ mass was ranked as follows: spring (60.2%) > fall (56.7%) \approx summer (56.6%) > winter (51.7%). The concentration of SNA was the highest in winter ($27.06 \mu\text{g}\cdot\text{m}^{-3}$), followed by spring ($16.43 \mu\text{g}\cdot\text{m}^{-3}$), fall ($11.38 \mu\text{g}\cdot\text{m}^{-3}$), and summer ($6.48 \mu\text{g}\cdot\text{m}^{-3}$), which contributed 87.4%, 88.4%, 79.7%, and 65.0% to TWSIs, respectively. SO_4^{2-} showed the same seasonal trends as SNA, which were not consistent with those of SO_2 : winter > fall > summer > spring. The reason for the highest SO_4^{2-} concentration in winter may be attributed to the formation of abundant precursor SO_2 through heterogeneous aqueous processes reaction. It is noteworthy that SO_2 concentration in spring was 1.6 times lower than that in fall, while the concentration of SO_4^{2-} in spring was 1.5 times higher than that in fall. Compared with the meteorological data (Table 1), it was found that the solar radiation and temperature were stronger in spring than in fall, which was conducive to the formation of SO_4^{2-} through a homogeneous gas phase oxidation reaction. The concentration of NO_3^- in winter was 2.3–8.1 times higher than in other seasons. However, there were little differences in the seasonal concentrations of its precursor NO_2 , with their concentrations 1.3–1.6 times higher in spring and winter than in other seasons. The variation of NO_3^- concentration in particulate matter largely depends on temperature and RH [45]. High temperature and low RH in summer are not conducive to the existence of NO_3^- in the form of particulate matter and also cause the loss of NO_3^- volatilization in the sampled filter membrane [37,39]. The low temperature and high RH in winter are beneficial for nitrate stabilization. NH_3 , mostly from agricultural emissions due to the intensive use of fertilizer, had higher concentrations in spring ($18.86 \mu\text{g}\cdot\text{m}^{-3}$) and summer ($14.57 \mu\text{g}\cdot\text{m}^{-3}$) than in fall ($11.98 \mu\text{g}\cdot\text{m}^{-3}$) and winter ($11.65 \mu\text{g}\cdot\text{m}^{-3}$). Abundant acidic substances in winter were conducive to the conversion of NH_3 to NH_4^+ , while high temperature and precipitation scavenging in summer decreased NH_4^+ , leading to a significantly higher concentration of NH_4^+ in winter than in summer.

Na^+ was another important ion and ranked fourth concentration in WSIs. Mg^{2+} and Ca^{2+} usually come from soil dust, and Na^+ can also come from sea salt in addition to soil dust [46]. In this study, the concentrations of Na^+ , Ca^{2+} , and Mg^{2+} were higher in summer than in other seasons, which may be related to the dust from the surrounding construction sites. K^+ and Cl^- concentrations were highest in winter, followed by spring and fall, and lowest in summer. K^+ is a representative element of biomass combustion, which reflects the phenomenon of straw and leaf burning in winter. Cl^- comes not only from biomass burning and fossil fuel burning but also from sea salt [47]. There was a significant correlation between K^+ and Cl^- in winter, $r = 0.97$. Considering that Wanzhou does not use coal for central heating in winter and is located away from the coast, biomass burning was likely to be the main cause of higher Cl^- concentrations in winter.

3.3. Stoichiometric Analysis of Cations and Anions

Figure 3 depicts the linear relationship between cations and anions equivalents in four seasons in Wanzhou. Anion equivalent (AE) and cation equivalent (CE) were calculated as follows:

$$\text{AE} = \frac{\text{Cl}^-}{35.5} + \frac{\text{SO}_4^{2-}}{48} + \frac{\text{NO}_3^-}{62} \quad (1)$$

$$\text{CE} = \frac{\text{Mg}^{2+}}{12} + \frac{\text{NH}_4^+}{18} + \frac{\text{Ca}^{2+}}{20} + \frac{\text{Na}^+}{23} + \frac{\text{K}^+}{39} \quad (2)$$

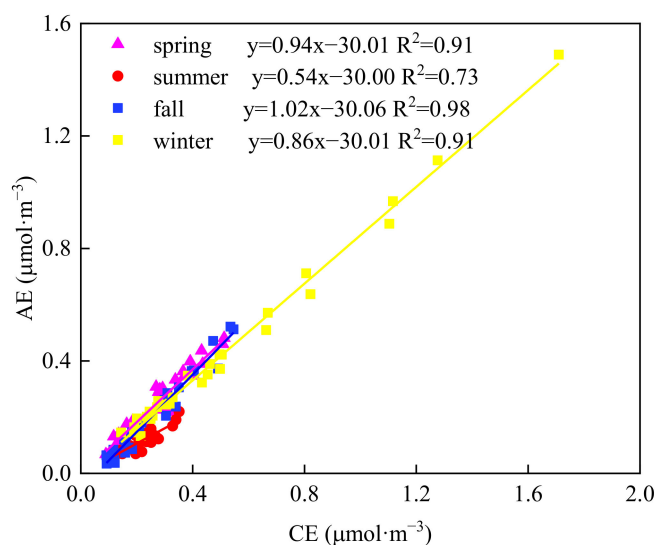


Figure 3. Plot of cations concentration vs. anions concentration in four seasons.

As shown in Figure 3, strong correlations between AE and CE were found in all seasons, supporting that the measured eight ions were the major constituents in the $\text{PM}_{2.5}$ ionic components. The annual mean AE/CE ratio (slope of the linear regression) was 0.90, indicating weak alkaline $\text{PM}_{2.5}$ aerosols at Wanzhou. Similar patterns of $\text{PM}_{2.5}$ acidity (AE/CE slope < 1) were also observed in Fuling and Beibei, both small cities of Chongqing [7,37]. Seasonally, except for fall, the slopes of the line for spring, summer, and winter were lower than 1. In summer, the slope of the line was 0.54, demonstrating an apparent deficiency of anions of $\text{PM}_{2.5}$ samples, which can be attributed partly to the measurement of bicarbonate and carbonate as well as the elevated concentrations of alkaline dust particles in summer, such as Na^+ and Ca^{2+} ; thus $\text{PM}_{2.5}$ samples showed alkaline feature. In spring and winter, the slopes of the line were 0.94 and 0.86, respectively, indicating a weakly alkaline property, which can be ascribed to the high levels of acid ions of SO_4^{2-} and NO_3^- in spring and winter. In the fall, most of the samples generally showed a balance between anions and cations, and the slope of the line was almost equal to 1.

3.4. Formation Path of SO_4^{2-} and NO_3^-

NO_3^- and SO_4^{2-} are mainly secondary ions formed by gaseous precursors (NO_x , SO_2) through atmospheric chemical reactions. The mass ratio of $\text{NO}_3^-/\text{SO}_4^{2-}$ is commonly used to assess the relative influence of mobile or stationary sources on atmospheric nitrogen and sulfur [33]. The high values of $\text{NO}_3^-/\text{SO}_4^{2-}$ (>1) are ascribed to the large number of mobile sources (such as motor vehicle exhaust) in China. If the $\text{NO}_3^-/\text{SO}_4^{2-}$ ratios are low (<1), that indicates that a fixed source (such as coal combustion) is the main source. During the sampling period, the annual average ratio of $\text{NO}_3^-/\text{SO}_4^{2-}$ in Wanzhou was 0.54, lower than Nanjing (1.38) and Shanghai (1.40) [48] and comparable with Fuling (0.49) [37]. The results indicated that the contribution of stationary sources to $\text{PM}_{2.5}$ was greater than that of mobile sources in Wanzhou. In addition, the seasonal average ratios of $\text{NO}_3^-/\text{SO}_4^{2-}$ were ranked in the order of winter (0.85) $>$ fall (0.57) $>$ spring (0.44) $>$ summer (0.27). The NO_x from automobile exhaust is more easily converted into NO_3^- under the poor atmospheric dilution and diffusion conditions in winter, which increases the concentration of NO_3^- in the atmosphere [5,45], thus resulting in the highest $\text{NO}_3^-/\text{SO}_4^{2-}$ ratio in winter. On the contrary, the minimum ratio appeared in summer, which may be related to the volatility of nitrate at high temperature [18].

Sulfur oxidation ratio (SOR) and nitrogen oxidation ratio (NOR) are usually used to represent the formation and transformation process of secondary aerosols using the following equations [49]:

$$\text{SOR} = \frac{[\text{SO}_4^{2-}]}{[\text{SO}_4^{2-}] + [\text{SO}_2]} \quad (3)$$

$$\text{NOR} = \frac{[\text{NO}_3^-]}{[\text{NO}_3^-] + [\text{NO}_2]} \quad (4)$$

where $[\text{SO}_4^{2-}]$, $[\text{SO}_2]$, $[\text{NO}_3^-]$, and $[\text{NO}_2]$ are the molar concentrations of SO_4^{2-} , SO_2 , NO_3^- and NO_2 , respectively. Because of the monitoring instrument failure, NO_2 and SO_2 data in the summer were missing. Generally, the critical values of SOR and NOR are both 0.1, and higher NOR and SOR values indicate increased secondary transformation [50,51]. During the sampling period, the average value of SOR was 0.31, indicating a significant secondary transformation of SO_2 in the atmosphere. In addition, the value of SOR was the highest in spring (0.40), followed by winter (0.30), and the lowest in fall (0.22). The NOR values had a different seasonal pattern from SOR, which peaked in winter (0.13) and had lower values in spring and fall (both 0.06). Both sulfate and nitrate had two formation pathways, homogenous and heterogeneous reactions. Homogeneous gas-phase oxidation reaction involves SO_2 or NO_2 and OH radicals, which is a strong function of temperature. Heterogeneous transformation processes ($\text{H}_2\text{O}_2/\text{O}_3$ oxidation under the catalysis of metal or hydrolysis of N_2O_5 on preexisting particles) are correlated with RH and mass concentration of particulate matter [7,18,52]. As shown in Figure 4a, when the temperature was low ($<15^\circ\text{C}$), its concentration increased with the temperature, but when the temperature was higher than 15°C , its concentration decreased rapidly, and NOR also presented a similar trend (Figure 4c). In winter, the temperature was usually below 15°C , and it was found that NH_4^+ and NO_3^- had significant correlation ($r = 0.84, 0.92, 0.95$ in spring, fall, and winter, respectively), so it can be inferred that NO_3^- was mainly formed through homogeneous meteorological reaction in winter. NO_3^- is more volatile at high temperatures, which is the reason NOR is lower at high temperatures [41]. Additionally, NOR increased with RH (Figure 4d), suggesting the main formation pathway of NO_3^- was a heterogeneous reaction in the fall (average RH: 83.3%). Since SOR increased with temperature and RH (Figure 4c,d), it can be speculated that SO_4^{2-} was mainly formed by heterogeneous reactions in winter (lower temperature, higher relative humidity, Table 1), while both homogeneous and heterogeneous reactions existed in spring and fall.

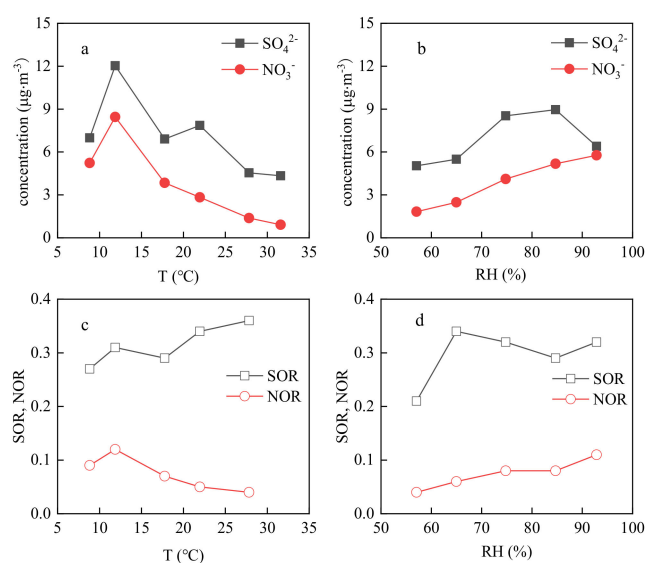


Figure 4. Evolution characteristics of SO_4^{2-} and NO_3^- (a,b) and their conversion rates (SOR and NOR) (c,d) with temperature and humidity.

3.5. Chemical Forms of SNA

NH_3 could react with acidic gases such as H_2SO_4 and HNO_3 to form $(\text{NH}_4)_2\text{SO}_4$, NH_4HSO_4 , and NH_4NO_3 through homogeneous reactions. Moreover, NH_3 reacts preferentially with H_2SO_4 to form non-volatile $(\text{NH}_4)_2\text{SO}_4$ or NH_4HSO_4 , and the excess NH_3 further reacts with HNO_3 to form relatively volatile NH_4NO_3 [53]. As shown in Figure 5, significant correlations between $[\text{NH}_4^+]$ and $[\text{SO}_4^{2-}]$ were found in the four seasons, with the correlation coefficient being larger than 0.90. The slopes of linear regressions higher than 2.0 indicated that there was sufficient NH_4^+ to neutralize SO_4^{2-} to form $(\text{NH}_4)_2\text{SO}_4$ rather than NH_4HSO_4 . In order to identify the specific existence forms of $(\text{NH}_4)_2\text{SO}_4$ or NH_4HSO_4 and NH_4NO_3 , it can be distinguished by comparing the NH_4^+ measured experimentally with the NH_4^+ calculated [54]. When NO_3^- , SO_4^{2-} and NH_4^+ exist as the form of $(\text{NH}_4)_2\text{SO}_4$ and NH_4NO_3 , the estimated concentration of NH_4^+ can be calculated by $\rho(\text{NH}_4^+) (\mu\text{g} \cdot \text{m}^{-3}) = 0.38\rho(\text{SO}_4^{2-}) + 0.29\rho(\text{NO}_3^-)$. When NO_3^- , SO_4^{2-} and NH_4^+ exist in the form of NH_4HSO_4 and NH_4NO_3 , the estimated concentration of NH_4^+ can be expressed as $\rho(\text{NH}_4^+) (\mu\text{g} \cdot \text{m}^{-3}) = 0.192\rho(\text{SO}_4^{2-}) + 0.29\rho(\text{NO}_3^-)$. The regression analysis of NH_4^+ measured and calculated values were shown in Table 3. Assuming that NH_4^+ existed in $(\text{NH}_4)_2\text{SO}_4$, the slopes of regression lines in spring, summer, fall, and winter were 0.99, 1.03, 0.93, and 1.21, respectively. When NH_4^+ was assumed to exist as the form of NH_4HSO_4 , the slopes of regression lines were 1.57, 1.74, 1.48, and 1.83, respectively. By comparison, the slopes of $(\text{NH}_4)_2\text{SO}_4$ in the four seasons were closer to 1, and the measured values and the calculated values were relatively consistent. Therefore, it can be concluded that NO_3^- , SO_4^{2-} , and NH_4^+ mainly exist in the form of $(\text{NH}_4)_2\text{SO}_4$ and NH_4NO_3 in Wanzhou during the sampling period.

Table 3. Regression analysis between calculated values and measured values of NH_4^+ .

Season	In the Form of $(\text{NH}_4)_2\text{SO}_4$			In the Form of NH_4HSO_4		
	Linear Regression Equation	R^2	p	Linear Regression Equation	R^2	p
Spring	$y = 0.99x - 0.54$	0.98	<0.01	$y = 1.57x - 0.52$	0.98	<0.01
Summer	$y = 1.04x - 0.74$	0.97		$y = 1.74x - 0.71$	0.93	
Fall	$y = 0.93x - 0.39$	0.99		$y = 1.48x - 0.42$	0.98	
Winter	$y = 1.21x - 1.02$	0.99		$y = 1.83x - 1.38$	0.99	

x represents NH_4^+ measured value ($\mu\text{g} \cdot \text{m}^{-3}$); y represents NH_4^+ calculated value ($\mu\text{g} \cdot \text{m}^{-3}$).

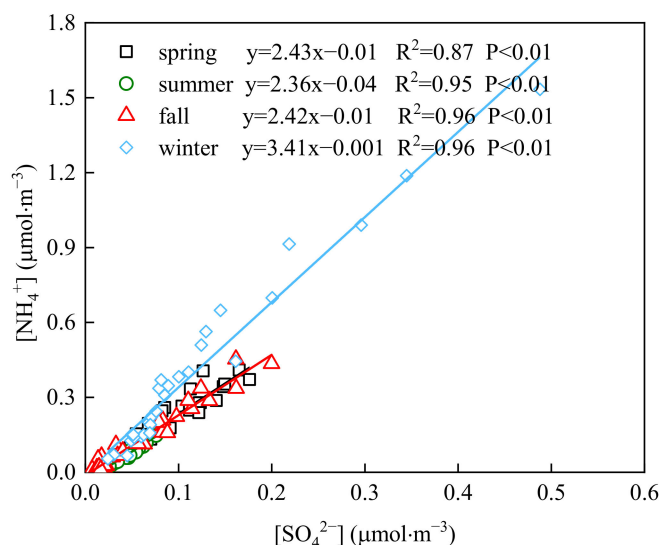


Figure 5. Correlations between [NH₄⁺] and [SO₄²⁻].

3.6. Source Apportionment of WSIs

3.6.1. Principal Component Analysis (PCA) of WSIs

In this study, principal component analysis (PCA) was used to analyze the sources of WSIs during the observation period. PCA can extract several potential factors from the mass concentration data, which can be used to explain the relationship between the measured samples [55]. PCA was conducted for 11 variables (Na⁺, NH₄⁺, K⁺, Mg²⁺, Ca²⁺, Cl⁻, NO₃⁻, SO₄²⁻, NH₃, SO₂, NO₂), and the KMO test value was 0.753, greater than 0.5, indicating that it was suitable for factor analysis. Based on the PCA method, three factors (potential sources) were identified as principal components (PC) at Wanzhou (Table 4). PC1 explained 49.5% of the total variance, and was mainly affected by NH₄⁺ (0.96), K⁺ (0.98), Cl⁻ (0.95), NO₃⁻ (0.89), SO₄²⁻ (0.96), NO₂ (0.56), and SO₂ (0.65). NH₄⁺, NO₃⁻, and SO₄²⁻ are the typical traces of secondary sources [56,57]. K⁺ and Cl⁻ are associated with coal combustion and biomass burning. SO₂ and NO₂ are derived from coal burning and automobile exhaust emissions, respectively. Therefore, PC1 was attributed to the mixture of secondary origin aerosol, biomass burning, coal combustion, and automobile exhaust. PC2, responsible for 23.2% of the total variance, was characterized by high loadings of Na⁺ (0.87), Mg²⁺ (0.70), and Ca²⁺ (0.86). Since Na⁺, Mg²⁺, and Ca²⁺ are principal markers of dust emissions [58,59], PC2 was identified as construction dust and road dust source in the present study. PC3 explained 9.68% of the total variance with obvious loading of NH₃ (0.93) and NH₃, which mainly came from agriculture activities. In view of there being several agricultural fields to the west of the sampling site, PC3 was regarded as agricultural activity.

Table 4. Results of principal component analysis.

	PCA Source Loadings		
	PC1	PC2	PC3
Na ⁺	0.13	0.87	-0.05
NH ₄ ⁺	0.96	-0.04	0.16
K ⁺	0.98	0.07	0.02
Mg ²⁺	0.33	0.70	-0.52
Ca ²⁺	-0.21	0.86	0.03
Cl ⁻	0.95	0.01	-0.06
NO ₃ ⁻	0.89	-0.03	0.29
SO ₄ ²⁻	0.96	-0.01	0.03
NH ₃	0.19	-0.08	0.93
NO ₂	0.56	-0.44	0.27

Table 4. Cont.

	PCA Source Loadings		
	PC1	PC2	PC3
SO ₂	0.65	0.12	−0.34
Variance	49.53%	23.16%	9.68%
Cumulative	49.53%	72.69%	82.37%

3.6.2. Regional Transport

To analyze the effects of air mass on atmospheric quality, 72 h backward trajectories arriving in Wanzhou during the sampling period were calculated by the TrajStat [60]. The starting time of trajectory calculation per day was 10:00 am (UTC), with the arrival level at 500 m AGL (Above Ground Level). The cluster analysis was based on the 72 h backward trajectories and grouped into five clusters (Figure 6). Cluster 1 mainly came from the southwest pathway, originating from Burma, through the Yunnan Province, and the junction of Chongqing and Guizhou Province. Cluster 3 represented the southern pathway which originated from Guangxi Province and passed through Guizhou Province. Clusters 1 and 3 (accounting for 8.8% and 17.7%, respectively) had mid-distance air mass trajectories and carried with the lowest PM_{2.5} and WSIs concentrations. However, Clusters 1 and 3 showed high proportions of dust ions (Na⁺, Mg²⁺, and Ca²⁺), accounting for 22.3% and 25.5%, respectively. In terms of the origins and pathways, these air masses were expected to bring in relatively clean air passing through some sparsely populated, thus contributing toward pollution alleviation in Wanzhou. Cluster 2 was the dominant trajectory in Wanzhou (accounting for 63.7%), which mainly originated from the local southeastern area. Since Wanzhou's large-scale industrial complexes, including chemical plants, cement plants, and power plants, are located southeast of the sampling site, the southeast wind brought in a large number of pollutants from the industrial activities from this region's sources [61]. Cluster 5 (accounting for 7.9%) had long-range air masses originating from southern Xinjiang Province through the Tibet Autonomous Region, Qinghai, and Sichuan Provinces. The air masses in Clusters 2 and 5 carried higher concentrations of PM_{2.5} and WSIs, and their ionic compositions were similar, with the proportion of SNA reaching 84.8% and 85.6% of WSIs, respectively. Cluster 4 (accounting for 1.8%) reflected the ultra-long-distance and polluted air masses transported from Saudi Arabia. This cluster corresponded to the highest concentrations of PM_{2.5} and WSIs, with the highest contribution (average 87.3%) from SNA. Since Cluster 4 mainly occurred in winter, it can be inferred that the transport of air mass from this pathway may be related to the air pollution in winter.

3.7. Air Pollution Event

There was a long-lasting pollution event that occurred from 31 December 2016 to 5 January 2017, with average PM_{2.5} concentration reaching 126.51 µg·m^{−3}, exceeding the NAAQS-China daily limit of 75 µg·m^{−3} by a factor of 1.8. The time series of daily meteorological parameters, gaseous precursors, PM_{2.5}, and WSIs concentrations are depicted in Figure 7. The whole sampling campaign was divided into three stages according to PM_{2.5} concentrations, namely, the pre-pollution stage (P1), the pollution occurred stage (P2), and the post-pollution stage (P3). The P1 phase was from 27 to 30 December 2016, when the average PM_{2.5}, NO₂, and SO₂ concentrations were 34.46, 46.25, and 14.00 µg·m^{−3}. The P2 phase covered the period (31 December 2016 to 5 January 2017) of the long-lasting pollution event, when the average PM_{2.5}, NO₂, and SO₂ concentrations were 126.51, 52.83, and 22.33 µg·m^{−3}. Compared with those in P1, the temperature and relative humidity increased by 23% and 17%, respectively, while the wind speed decreased from 0.71 to 0.62 m·s^{−1}. During this period, PM_{2.5} gradually accumulated and peaked on 4 January 2017 to the level of 156.30 µg·m^{−3}, while NO₂ and SO₂ peaked at 65 and 26 µg·m^{−3} on 31 December 2016, and 2 January 2017, respectively. The P3 phase was from 6 to 7 January 2017, when PM_{2.5} concentration decreased rapidly due to the removal of air pollutants by rainfall.

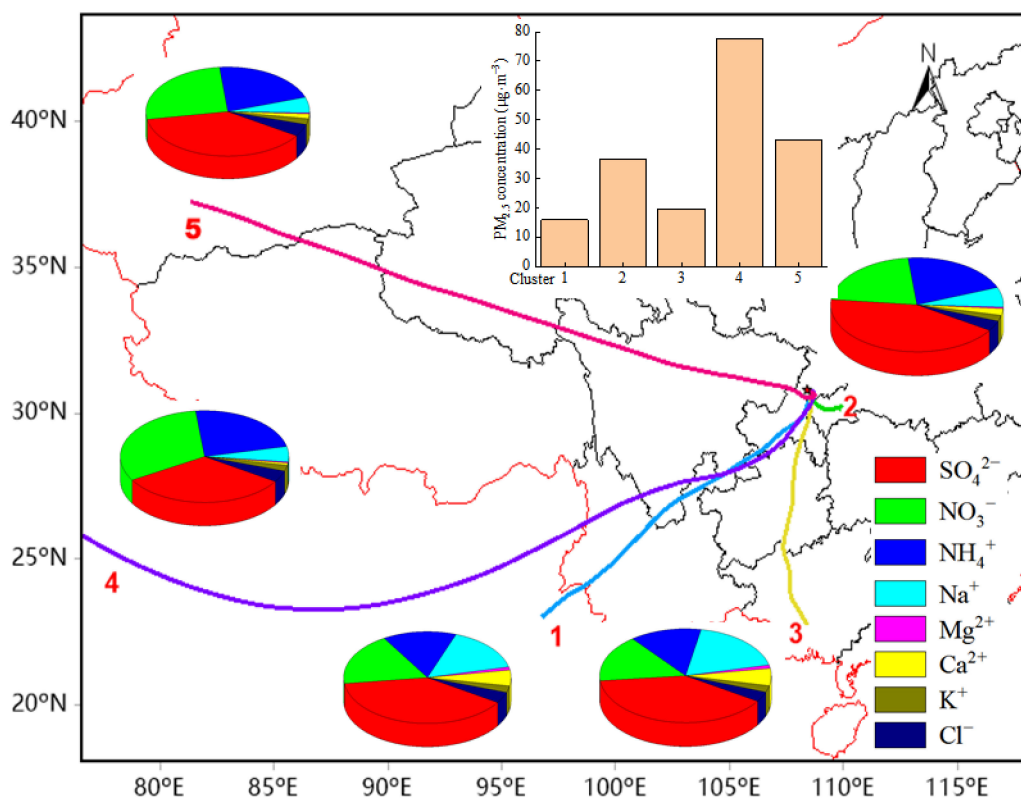


Figure 6. 72 h backward trajectories clusters in Wanzhou during the observation period.

As shown in Figure 7, the concentrations of $PM_{2.5}$, WSIS, and all the measured gaseous precursors were observably higher during the pollution phase (P2) than before (P1) and after the pollution event (P3). Taking P1 as the reference phase, $PM_{2.5}$ concentration in P2 increased 3.7 times, and the total amount of SNA increased 4.5 times. SO_4^{2-} , NO_3^- , and NH_4^+ increased 4.3, 4.1, and 5.3 times, from a low of 6.13, 4.28, and 3.23 $\mu\text{g}\cdot\text{m}^{-3}$ (P1) to 26.37, 17.23, and 17.12 $\mu\text{g}\cdot\text{m}^{-3}$ (P2), respectively. SOR and NOR were also enhanced by a factor of 1.8 and 2.8 in P2, respectively (from 0.24 to 0.42, 0.07 to 0.20, respectively). However, their gaseous precursors SO_2 and NO_2 only increased by 1.6 and 1.1 times in P2, respectively. It is evident that this air pollution event was mainly caused by the enhanced chemical transformation of gaseous precursors to SNA. Compared to P1, the temperature increased by 1.2 °C in P2 (from 9.26 to 11.41 °C), which promoted stronger photochemical reactions. A good correlation was found between temperature and SOR ($r = 0.65$) or NOR ($r = 0.85$), suggesting homogeneous reactions as the main formation mechanism for the high level of SO_4^{2-} and NO_3^- . At the same time, the average relative humidity increased from 71% in P1 to 83% in P2. The relative humidity also had a good correlation with SOR and NOR, and the correlation coefficients were 0.73 and 0.95, respectively, indicating that heterogeneous reaction also contributed to the increase of SO_4^{2-} and NO_3^- concentrations. The strong enhancement of NH_4^+ concentration in P2 was apparently attributed to those of SO_4^{2-} and NO_3^- . In addition, the concentration of K^+ and Cl^- also increased significantly during the P2 stage, which increased by 3.6 and 4.7 times, respectively, but the proportion of K^+ and Cl^- in WSIS varied little. The elevated concentration of K^+ and Cl^- may be related to straw burning in the surrounding farmland. The concentrations of Na^+ , Mg^{2+} , and Ca^{2+} did not vary significantly during the whole sampling period, indicating that the source strength was relatively stable. Combined with the little variation of concentration of primary pollutants SO_2 and NO_2 , it can be inferred that this air pollution event was mostly caused by the enhanced formation of SNA through homogeneous and heterogeneous reactions.

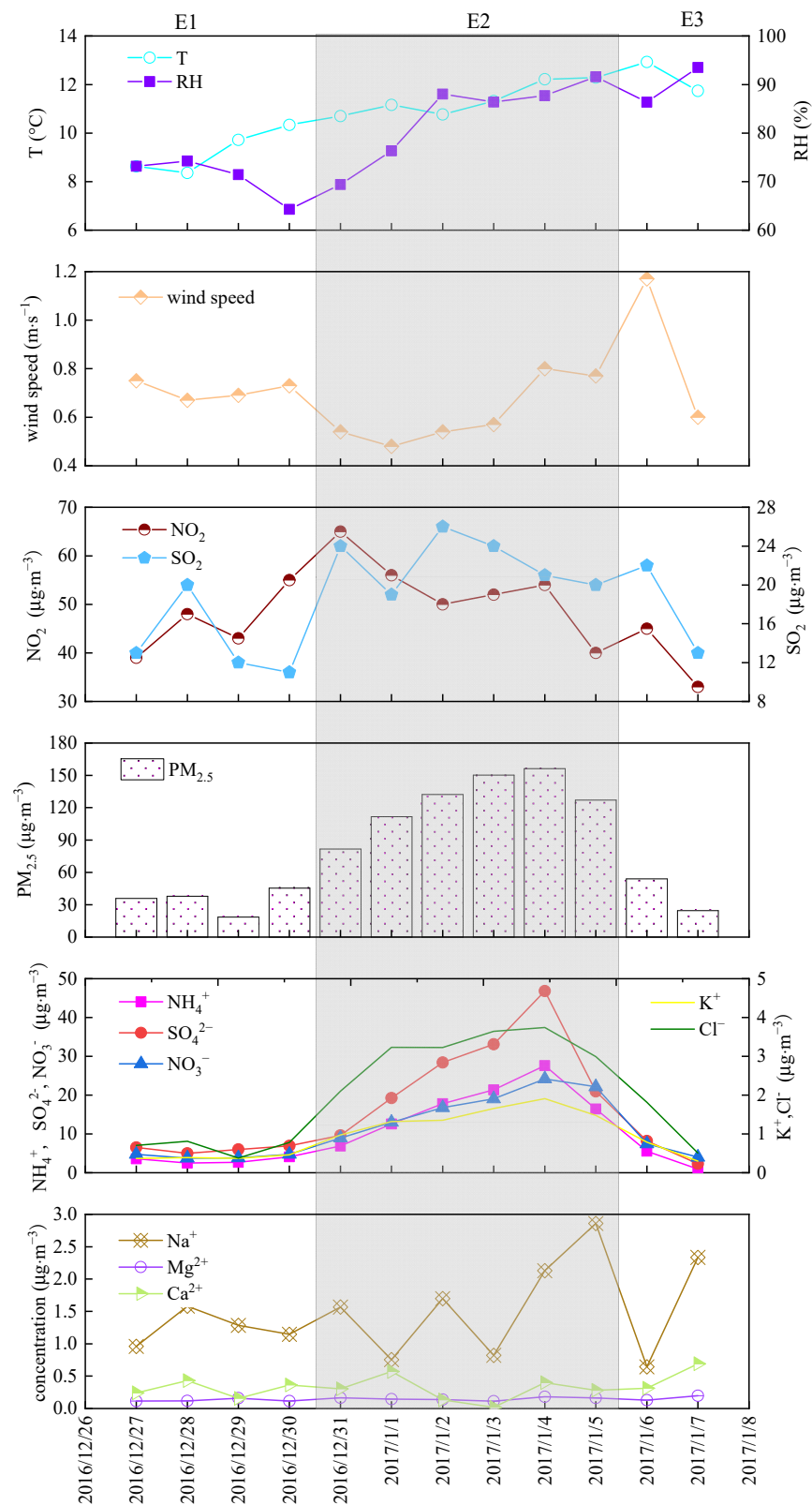


Figure 7. The time series of daily meteorological parameters, gaseous precursors, PM_{2.5}, and WSIs concentrations from 27 December 2016 to 7 January 2017.

4. Conclusions

From April 2016 to January 2017, PM_{2.5} samples were collected in four months (each month represented a season) to analyze the characteristics and sources of WSIs in Wanzhou. Statistical results displayed that the annual average value in Wanzhou was 33.38 $\mu\text{g}\cdot\text{m}^{-3}$, which was lower than the National Ambient Air Quality Standards of China (NAAQS-China, annual limit of 35 $\mu\text{g}\cdot\text{m}^{-3}$). SO_4^{2-} , NO_3^- , and NH_4^+ were the dominating water-soluble ions, with corresponding percentage contributions to the total WSIs of 41.1%, 22.1%, and 19.9%, respectively. PM_{2.5} and WSIs showed the highest concentrations in winter and lowest concentrations in summer. Ion balance analysis showed that PM_{2.5} was alkaline in summer, weakly alkaline in spring and winter, and close to neutral in fall. The annual average ratio of $\text{NO}_3^-/\text{SO}_4^{2-}$ in Wanzhou was 0.54, demonstrating that the contribution of stationary sources to PM_{2.5} was greater than that of mobile sources in Wanzhou. NO_3^- was mainly formed through homogeneous meteorological reactions in winter and heterogeneous reactions in fall. SO_4^{2-} was mainly formed by heterogeneous reactions in winter, while both homogeneous and heterogeneous reactions existed in spring and fall. NO_3^- , SO_4^{2-} , and NH_4^+ mainly exist in the form of $(\text{NH}_4)_2\text{SO}_4$ and NH_4NO_3 in Wanzhou during the sampling period. Three main sources of WSIs in PM_{2.5} in Wanzhou were analyzed by PCA, which were the mixture of secondary origin aerosol, biomass burning, coal combustion, construction dust and road dust, and agriculture activities, respectively. The 72 h backward trajectory analysis indicated that the local emissions had a significant influence on the atmosphere of Wanzhou, and the ultra-long-distance transport from the southwest air masses carrying the highest PM_{2.5} and WSIs may cause air pollution in winter. An air pollution event that occurred in winter was mostly caused by the enhanced formation of SNA through homogeneous and heterogeneous reactions.

Author Contributions: Conceptualization, Y.H. and L.Z.; methodology, L.Z.; writing—original draft preparation, Y.H.; writing—review and editing, F.Y., T.L. and L.Z.; visualization, Y.C.; supervision, C.P.; funding acquisition, Y.H. and L.Z. All authors have read and agreed to the published version of the manuscript.

Funding: This research was funded by the Scientific and Technological Research Program of Chongqing Municipal Education Commission, grant number KJQN202001232 and KJQN202101201, and Key Laboratory of Water Environment Evolution and Pollution Control in Three Gorges Reservoir.

Institutional Review Board Statement: Not applicable.

Informed Consent Statement: Not applicable.

Data Availability Statement: All data presented in this paper are available upon request to Yimin Huang (huangyimin_1986@126.com).

Conflicts of Interest: The authors declare no conflict of interest.

References

1. He, Q.; Yan, Y.; Guo, L.; Zhang, Y.; Zhang, G.; Wang, X. Characterization and source analysis of water-soluble inorganic ionic species in PM_{2.5} in Taiyuan city, China. *Atmos. Res.* **2017**, *184*, 48–55. [[CrossRef](#)]
2. Huang, R.-J.; Zhang, Y.; Bozzetti, C.; Ho, K.-F.; Cao, J.-J.; Han, Y.; Daellenbach, K.R.; Slowik, J.G.; Platt, S.M.; Canonaco, F.; et al. High secondary aerosol contribution to particulate pollution during haze events in China. *Nature* **2014**, *514*, 218–222. [[CrossRef](#)] [[PubMed](#)]
3. Wang, W.; Primbs, T.; Tao, S.; Simonich, S.L.M. Atmospheric Particulate Matter Pollution during the 2008 Beijing Olympics. *Environ. Sci. Technol.* **2009**, *43*, 6440. [[CrossRef](#)]
4. Hu, G.; Zhang, Y.; Sun, J.; Zhang, L.; Shen, X.; Lin, W.; Yang, Y. Variability, formation and acidity of water-soluble ions in PM_{2.5} in Beijing based on the semi-continuous observations. *Atmos. Res.* **2014**, *145–146*, 1–11. [[CrossRef](#)]
5. Tian, M.; Wang, H.; Chen, Y.; Zhang, L.; Shi, G.; Liu, Y.; Yu, J.; Zhai, C.; Wang, J.; Yang, F. Highly time-resolved characterization of water-soluble inorganic ions in PM_{2.5} in a humid and acidic mega city in Sichuan Basin, China. *Sci. Total Environ.* **2016**, *580*, 224–234. [[CrossRef](#)]
6. Zheng, S.; Pozzer, A.; Cao, C.X.; Lelieveld, J. Long-term (2001–2012) concentrations of fine particulate matter (PM_{2.5}) and the impact on human health in Beijing, China. *Atmos. Chem. Phys.* **2015**, *15*, 5715–5725. [[CrossRef](#)]

7. Pan, Y.; Luo, L.; Xiao, H.; Zheng, N.; Fang, X.; Zhang, Z.; Xiao, H. A one-year comprehensive characteristics of water soluble inorganic ions in PM_{2.5} from a typical mountainous city. *Atmos. Pollut. Res.* **2020**, *11*, 1883–1890. [[CrossRef](#)]
8. Chen, Y.; Xie, S.-D.; Luo, B.; Zhai, C.-Z. Particulate pollution in urban Chongqing of southwest China: Historical trends of variation, chemical characteristics and source apportionment. *Sci. Total Environ.* **2017**, *584–585*, 523–534. [[CrossRef](#)]
9. Wang, H.; Tian, M.; Chen, Y.; Shi, G.; Liu, Y.; Yang, F.; Zhang, L.; Deng, L.; Yu, J.; Peng, C.; et al. Seasonal characteristics, formation mechanisms and source origins of PM_{2.5} in two megacities in Sichuan Basin, China. *Atmos. Chem. Phys.* **2018**, *18*, 865–881. [[CrossRef](#)]
10. Tian, M.; Wang, H.; Chen, Y.; Yang, F.M.; Zhang, X.H.; Zou, Q.; Zhang, R.Q.; Ma, Y.L.; He, K.B. Characteristics of aerosol pollution during heavy haze events in Suzhou, China. *Atmos. Chem. Phys.* **2016**, *16*, 7357–7371. [[CrossRef](#)]
11. Quan, J.; Tie, X.; Zhang, Q.; Liu, Q.; Li, X.; Gao, Y.; Zhao, D. Characteristics of heavy aerosol pollution during the 2012–2013 winter in Beijing, China. *Atmos. Environ.* **2014**, *88*, 83–89. [[CrossRef](#)]
12. Wang, S.; Yin, S.; Zhang, R.; Yang, L.; Zhao, Q.; Zhang, L.; Yan, Q.; Jiang, N.; Tang, X. Insight into the formation of secondary inorganic aerosol based on high-time-resolution data during haze episodes and snowfall periods in Zhengzhou, China. *Sci. Total Environ.* **2019**, *660*, 47–56. [[CrossRef](#)]
13. Ye, S.; Ma, T.; Duan, F.; Li, H.; He, K.; Xia, J.; Yang, S.; Zhu, L.; Ma, Y.; Huang, T.; et al. Characteristics and formation mechanisms of winter haze in Changzhou, a highly polluted industrial city in the Yangtze River Delta, China. *Environ. Pollut.* **2019**, *253*, 377–383. [[CrossRef](#)]
14. Wang, Y.; Zhuang, G.; Zhang, X.; Huang, K.; Xu, C.; Tang, A.; Chen, J.; An, Z. The ion chemistry, seasonal cycle, and sources of PM_{2.5} and TSP aerosol in Shanghai. *Atmos. Environ.* **2006**, *40*, 2935–2952. [[CrossRef](#)]
15. Tan, J.-H.; Duan, J.-C.; Chen, D.-H.; Wang, X.-H.; Guo, S.-J.; Bi, X.-H.; Sheng, G.-Y.; He, K.-B.; Fu, J.-M. Chemical characteristics of haze during summer and winter in Guangzhou. *Atmos. Res.* **2009**, *94*, 238–245. [[CrossRef](#)]
16. Yang, Y.; Zhou, R.; Yu, Y.; Yan, Y.; Liu, Y.; Di, Y.; Wu, D.; Zhang, W. Size-resolved aerosol water-soluble ions at a regional background station of Beijing, Tianjin, and Hebei, North China. *J. Environ. Sci.* **2017**, *55*, 146–156. [[CrossRef](#)]
17. Zhao, P.S.; Dong, F.; He, D.; Zhao, X.J.; Zhang, X.L.; Zhang, W.Z.; Yao, Q.; Liu, H.Y. Characteristics of concentrations and chemical compositions for PM_{2.5} in the region of Beijing, Tianjin, and Hebei, China. *Atmos. Chem. Phys.* **2013**, *13*, 4631–4644. [[CrossRef](#)]
18. Meng, C.; Wang, L.; Zhang, F.; Wei, Z.; Ma, S.; Ma, X.; Yang, J. Characteristics of concentrations and water-soluble inorganic ions in PM_{2.5} in Handan City, Hebei province, China. *Atmos. Res.* **2016**, *171*, 133–146. [[CrossRef](#)]
19. Zhou, H.; Lü, C.; He, J.; Gao, M.; Zhao, B.; Ren, L.; Zhang, L.; Fan, Q.; Liu, T.; He, Z.; et al. Stoichiometry of water-soluble ions in PM_{2.5}: Application in source apportionment for a typical industrial city in semi-arid region, Northwest China. *Atmos. Res.* **2018**, *204*, 149–160. [[CrossRef](#)]
20. Tao, J.; Zhang, L.; Cao, J.; Zhong, L.; Chen, D.; Yang, Y.; Chen, D.; Chen, L.; Zhang, Z.; Wu, Y.; et al. Source apportionment of PM_{2.5} at urban and suburban areas of the Pearl River Delta region, south China—With emphasis on ship emissions. *Sci. Total Environ.* **2016**, *574*, 1559–1570. [[CrossRef](#)]
21. Zhou, J.; Xing, Z.; Deng, J.; Du, K. Characterizing and sourcing ambient PM_{2.5} over key emission regions in China I: Water-soluble ions and carbonaceous fractions. *Atmos. Environ.* **2016**, *135*, 20–30. [[CrossRef](#)]
22. Zhao, J.; Zhang, F.; Xu, Y.; Chen, J. Characterization of water-soluble inorganic ions in size-segregated aerosols in coastal city, Xiamen. *Atmos. Res.* **2011**, *99*, 546–562. [[CrossRef](#)]
23. Xu, L.; Chen, X.; Chen, J.; Zhang, F.; He, C.; Zhao, J.; Yin, L. Seasonal variations and chemical compositions of PM_{2.5} aerosol in the urban area of Fuzhou, China. *Atmos. Res.* **2012**, *104–105*, 264–272. [[CrossRef](#)]
24. Tao, J.; Zhang, L.; Cao, J.; Zhang, R. A review of current knowledge concerning PM_{2.5} chemical composition, aerosol optical properties and their relationships across China. *Atmos. Chem. Phys.* **2017**, *17*, 9485–9518. [[CrossRef](#)]
25. Li, M.; Liu, H.; Geng, G.; Hong, C.; Liu, F.; Song, Y.; Tong, D.; Zheng, B.; Cui, H.; Man, H.; et al. Anthropogenic emission inventories in China: A review. *Natl. Sci. Rev.* **2017**, *4*, 834–866. [[CrossRef](#)]
26. Zhang, Y.; Tang, A.; Wang, C.; Ma, X.; Li, Y.; Xu, W.; Xia, X.; Zheng, A.; Li, W.; Fang, Z.; et al. PM_{2.5} and water-soluble inorganic ion concentrations decreased faster in urban than rural areas in China. *J. Environ. Sci.* **2022**, *122*, 83–91. [[CrossRef](#)]
27. Li, H.; Zhang, Q.; Zheng, B.; Chen, C.; Wu, N.; Guo, H.; Zhang, Y.; Zheng, Y.; Li, X.; He, K. Nitrate-driven urban haze pollution during summertime over the North China Plain. *Atmos. Chem. Phys.* **2018**, *18*, 5293–5306. [[CrossRef](#)]
28. Xu, Q.; Wang, S.; Jiang, J.; Bhattarai, N.; Li, X.; Chang, X.; Qiu, X.; Zheng, M.; Hua, Y.; Hao, J. Nitrate dominates the chemical composition of PM_{2.5} during haze event in Beijing, China. *Sci. Total Environ.* **2019**, *689*, 1293–1303. [[CrossRef](#)]
29. Fu, X.; Wang, T.; Gao, J.; Wang, P.; Liu, Y.; Wang, S.; Zhao, B.; Xue, L. Persistent Heavy Winter Nitrate Pollution Driven by Increased Photochemical Oxidants in Northern China. *Environ. Sci. Technol.* **2020**, *54*, 3881–3889. [[CrossRef](#)]
30. Li, H.; Zhang, Q.; Zhang, Q.; Chen, C.; Wang, L.; Wei, Z.; Zhou, S.; Parworth, C.; Zheng, B.; Canonaco, F.; et al. Wintertime aerosol chemistry and haze evolution in an extremely polluted city of the North China Plain: Significant contribution from coal and biomass combustion. *Atmos. Chem. Phys.* **2017**, *17*, 4751–4768. [[CrossRef](#)]
31. Xu, J.-S.; Xu, M.; Snape, C.; He, J.; Behera, S.N.; Xu, H.-H.; Ji, D.-S.; Wang, C.; Yu, H.; Xiao, H.; et al. Temporal and spatial variation in major ion chemistry and source identification of secondary inorganic aerosols in Northern Zhejiang Province, China. *Chemosphere* **2017**, *179*, 316–330. [[CrossRef](#)] [[PubMed](#)]

32. Zheng, B.; Zhang, Q.; Zhang, Y.; He, K.B.; Wang, K.; Zheng, G.J.; Duan, F.K.; Ma, Y.L.; Kimoto, T. Heterogeneous chemistry: A mechanism missing in current models to explain secondary inorganic aerosol formation during the January 2013 haze episode in North China. *Atmos. Chem. Phys.* **2015**, *15*, 2031–2049. [[CrossRef](#)]
33. Ming, L.; Jin, L.; Li, J.; Fu, P.; Yang, W.; Liu, D.; Zhang, G.; Wang, Z.; Li, X. PM_{2.5} in the Yangtze River Delta, China: Chemical compositions, seasonal variations, and regional pollution events. *Environ. Pollut.* **2017**, *223*, 200–212. [[CrossRef](#)] [[PubMed](#)]
34. Chen, Y.; Xie, S. Temporal and spatial visibility trends in the Sichuan Basin, China, 1973 to 2010. *Atmos. Res.* **2012**, *112*, 25–34. [[CrossRef](#)]
35. Zhang, L.; Huang, Y.; Liu, Y.; Yang, F.; Lan, G.; Fu, C.; Wang, J. Characteristics of Carbonaceous Species in PM_{2.5} in Wanzhou in the Hinterland of the Three Gorges Reservoir of Northeast Chongqing, China. *Atmosphere* **2015**, *6*, 534–546. [[CrossRef](#)]
36. Huang, Y.; Zhang, L.; Qiu, Y.; Chen, Y.; Shi, G.; Li, T.; Zhang, L.; Yang, F. Five-year Record of Black Carbon Concentrations in Urban Wanzhou, Sichuan Basin, China. *Aerosol Air Qual. Res.* **2020**, *20*, 1282–1293. [[CrossRef](#)]
37. Qiao, B.; Chen, Y.; Tian, M.; Wang, H.; Yang, F.; Shi, G.; Zhang, L.; Peng, C.; Luo, Q.; Ding, S. Characterization of water soluble inorganic ions and their evolution processes during PM_{2.5} pollution episodes in a small city in southwest China. *Sci. Total Environ.* **2018**, *650*, 2605–2613. [[CrossRef](#)]
38. Peng, C.; Tian, M.; Chen, Y.; Wang, H.; Zhang, L.; Shi, G.; Liu, Y.; Yang, F.; Zhai, C. Characteristics, Formation Mechanisms and Potential Transport Pathways of PM_{2.5} at a Rural Background Site in Chongqing, Southwest China. *Aerosol Air Qual. Res.* **2019**, *19*, 1980–1992. [[CrossRef](#)]
39. Chen, Y.; Xie, S.-D.; Luo, B.; Zhai, C. Characteristics and Sources of Water-Soluble Ions in PM_{2.5} in the Sichuan Basin, China. *Atmosphere* **2019**, *10*, 78. [[CrossRef](#)]
40. Guo, W.; Long, C.; Zhang, Z.; Zheng, N.; Xiao, H.; Xiao, H. Seasonal Control of Water-Soluble Inorganic Ions in PM_{2.5} from Nanning, a Subtropical Monsoon Climate City in Southwestern China. *Atmosphere* **2019**, *11*, 5. [[CrossRef](#)]
41. Guo, W.; Zhang, Z.; Zheng, N.; Luo, L.; Xiao, H.; Xiao, H. Chemical characterization and source analysis of water-soluble inorganic ions in PM_{2.5} from a plateau city of Kunming at different seasons. *Atmos. Res.* **2019**, *234*, 104687. [[CrossRef](#)]
42. Liu, K.; Ren, J. Seasonal characteristics of PM_{2.5} and its chemical species in the northern rural China. *Atmos. Pollut. Res.* **2020**, *11*, 1891–1901. [[CrossRef](#)]
43. Ma, X.; Xiao, Z.; He, L.; Shi, Z.; Cao, Y.; Tian, Z.; Vu, T.; Liu, J. Chemical Composition and Source Apportionment of PM_{2.5} in Urban Areas of Xiangtan, Central South China. *Int. J. Environ. Res. Public Health* **2019**, *16*, 539. [[CrossRef](#)]
44. Zhang, L.; Tian, M.; Peng, C.; Fu, C.; Li, T.; Chen, Y.; Qiu, Y.; Huang, Y.; Wang, H.; Li, Z.; et al. Nitrogen wet deposition in the Three Gorges Reservoir area: Characteristics, fluxes, and contributions to the aquatic environment. *Sci. Total Environ.* **2020**, *738*, 140309. [[CrossRef](#)]
45. Pathak, R.K.; Louie, P.K.; Chan, C.K. Characteristics of aerosol acidity in Hong Kong. *Atmos. Environ.* **2004**, *38*, 2965–2974. [[CrossRef](#)]
46. Liu, J.; Wu, D.; Fan, S.; Mao, X.; Chen, H. A one-year, on-line, multi-site observational study on water-soluble inorganic ions in PM_{2.5} over the Pearl River Delta region, China. *Sci. Total Environ.* **2017**, *601–602*, 1720–1732. [[CrossRef](#)]
47. Li, X.; Wang, S.; Duan, L.; Hao, J.; Li, C.; Chen, Y.; Yang, L. Particulate and Trace Gas Emissions from Open Burning of Wheat Straw and Corn Stover in China. *Environ. Sci. Technol.* **2007**, *41*, 6052–6058. [[CrossRef](#)]
48. Du, W.; Hong, Y.-W.; Xiao, H.; Zhang, Y.; Chen, Y.; Xu, L.; Chen, J.; Deng, J. Chemical Characterization and Source Apportionment of PM_{2.5} during Spring and Winter in the Yangtze River Delta, China. *Aerosol Air Qual. Res.* **2017**, *17*, 2165–2180. [[CrossRef](#)]
49. Cheng, C.; Shi, M.; Liu, W.; Mao, Y.; Hu, J.; Tian, Q.; Chen, Z.; Hu, T.; Xing, X.; Qi, S. Characteristics and source apportionment of water-soluble inorganic ions in PM_{2.5} during a wintertime haze event in Huanggang, central China. *Atmos. Pollut. Res.* **2020**, *12*, 111–123. [[CrossRef](#)]
50. Zhang, R.; Sun, X.; Shi, A.; Huang, Y.; Yan, J.; Nie, T.; Yan, X.; Li, X. Secondary inorganic aerosols formation during haze episodes at an urban site in Beijing, China. *Atmos. Environ.* **2018**, *177*, 275–282. [[CrossRef](#)]
51. Kang, C.-M.; Lee, H.S.; Kang, B.-W.; Lee, S.-K.; Sunwoo, Y. Chemical characteristics of acidic gas pollutants and PM_{2.5} species during hazy episodes in Seoul, South Korea. *Atmos. Environ.* **2004**, *38*, 4749–4760. [[CrossRef](#)]
52. Seinfeld, J.H. ES&T Books: Atmospheric Chemistry and Physics of Air Pollution. *Environ. Sci. Technol.* **1986**, *20*, 863. [[CrossRef](#)]
53. Pathak, R.K.; Wu, W.S.; Wang, T. Summertime PM_{2.5} ionic species in four major cities of China: Nitrate formation in an ammonia-deficient atmosphere. *Atmos. Chem. Phys.* **2009**, *9*, 1711–1722. [[CrossRef](#)]
54. Shen, Z.; Arimoto, R.; Cao, J.; Zhang, R.; Li, X.; Du, N.; Okuda, T.; Nakao, S.; Tanaka, S. Seasonal Variations and Evidence for the Effectiveness of Pollution Controls on Water-Soluble Inorganic Species in Total Suspended Particulates and Fine Particulate Matter from Xi'an, China. *J. Air Waste Manag. Assoc.* **2008**, *58*, 1560–1570. [[CrossRef](#)]
55. Mukerjee, S.; Shadwick, D.S.; A Smith, L.; Somerville, M.C.; E Dean, K.; Bowser, J.J. Techniques to assess cross-border air pollution and application to a US-Mexico border region. *Sci. Total Environ.* **2001**, *276*, 205–224. [[CrossRef](#)]
56. Jain, S.; Sharma, S.K.; Choudhary, N.; Masiwal, R.; Saxena, M.; Sharma, A.; Mandal, T.K.; Gupta, A.; Gupta, N.C.; Sharma, C. Chemical characteristics and source apportionment of PM_{2.5} using PCA/APCS, UNMIX, and PMF at an urban site of Delhi, India. *Environ. Sci. Pollut. Res.* **2017**, *24*, 14637–14656. [[CrossRef](#)]
57. Liu, Z.; Xie, Y.; Hu, B.; Wen, T.; Xin, J.; Li, X.; Wang, Y. Size-resolved aerosol water-soluble ions during the summer and winter seasons in Beijing: Formation mechanisms of secondary inorganic aerosols. *Chemosphere* **2017**, *183*, 119–131. [[CrossRef](#)]

58. Agarwal, A.; Satsangi, A.; Lakhani, A.; Kumari, K.M. Seasonal and spatial variability of secondary inorganic aerosols in PM_{2.5} at Agra: Source apportionment through receptor models. *Chemosphere* **2019**, *242*, 125132. [[CrossRef](#)]
59. Saxena, M.; Sharma, A.; Sen, A.; Saxena, P.; Saraswati Mandal, T.; Sharma, S.; Sharma, C. Water soluble inorganic species of PM₁₀ and PM_{2.5} at an urban site of Delhi, India: Seasonal variability and sources. *Atmos. Res.* **2017**, *184*, 112–125. [[CrossRef](#)]
60. Wang, Y.Q.; Zhang, X.Y.; Draxler, R.R. TrajStat: GIS-based software that uses various trajectory statistical analysis methods to identify potential sources from long-term air pollution measurement data. *Environ. Model. Softw.* **2009**, *24*, 938–939. [[CrossRef](#)]
61. Huang, Y.; Liu, Y.; Zhang, L.; Peng, C.; Yang, F. Characteristics of Carbonaceous Aerosol in PM_{2.5} at Wanzhou in the Southwest of China. *Atmosphere* **2018**, *9*, 37. [[CrossRef](#)]